Relationship between edge localized mode severity and electron transport in the National Spherical Torus Experiment[a)]

K. Tritz,[1,b)] S. Kaye,[2] R. Maingi,[3] S. Sabbagh,[4] D. Stutman,[1] R. Bell,[2] L. Delgado-Aparicio,[1] C. W. Domier,[5] M. Finkenthal,[1] B. LeBlanc,[2] W. Lee,[6] N. C. Luhmann, Jr.,[5] E. Mazzucato,[2] H. Park,[2] and D. R. Smith[2]
[1]*The Johns Hopkins University, Baltimore, Maryland 21218, USA*
[2]*Princeton Plasma Physics Laboratory, Princeton, New Jersey 08543, USA*
[3]*Oak Ridge National Laboratory, Oak Ridge, Tennessee 37830, USA*
[4]*Columbia University, New York, New York, 10027, USA*
[5]*University of California at Davis, Davis, California 95616, USA*
[6]*Pohang University of Science and Technology, Pohang, Republic of Korea*

(Received 16 November 2007; accepted 5 March 2008; published online 5 May 2008)

In the National Spherical Torus Experiment [J. Menard *et al.*, Nucl. Fusion **47**, S645 (2007)], "giant" edge localized modes (ELMs) can occur resulting in a loss of plasma stored energy of up to 30%. These events are distinct from type I ELMs, whose energy loss is typically 4–10%, and they are accompanied by a cold pulse that causes a global decrease in the electron temperature profile. Estimates of the electron thermal transport during the cold pulses show a large enhancement over the underlying cross-field thermal diffusivity, χ_e, of up to several tens of m^2/s. Following the ELM, short-wavelength fluctuations increase in the plasma edge and core, corresponding to an increase in the electron temperature gradient from the propagating cold pulse. Fast electron temperature measurements indicate that the normalized electron temperature scale length, R/L_{Te}, reaches the threshold value for instability predicted by a fit to linear stability calculations. This is observed on time scales that match the growth of the high-k fluctuations in the plasma core, indicating that the enhanced χ_e and energy loss from the "giant" ELM appears to be related to critical gradient physics and the destabilization of electron temperature gradient modes. © *2008 American Institute of Physics*. [DOI: 10.1063/1.2902349]

I. INTRODUCTION

The understanding of edge localized modes (ELMs) and their effects is of great importance for the future of high-power fusion devices.[1] ELMs can appear in the high confinement mode (H-mode) discharges, and are often invoked as a mechanism to exhaust unwanted impurities from the edge of the plasma into the scrape off layer (SOL) and divertor region. Along with the ejection of impurity particles, the intermittent ELMs also cause the release of plasma stored energy which can range from $<1\%$ to several % of the plasma total stored energy, W_{tot}. Of particular interest are the larger, type I ELMs that appear in high-performance scenarios, such as those considered for baseline ITER operation.[2] While the present fusion devices can tolerate the energy loss from these events, type I ELMs in future high-power machines can cause a transient heat load on the plasma facing components (PFCs) that exceeds the power handling capabilities of the materials and have a severe impact on the lifetime of the PFCs and divertor components.[3]

On the National Spherical Torus Experiment (NSTX) device,[4] ELM behavior is similar to that of conventional, large aspect ratio machines, with a few exceptions. A small, type V ELM regime has been identified that combines the favorable edge density control and impurity particle handling properties of ELMs with a low transient peak heat flux. These ELMs would mitigate the demands on the PFC materials for future devices.[5] However, large events labeled "giant" ELMs have also been observed that correspond to a loss in plasma total stored energy of up to 30% on time scales of a few milliseconds.[6,7] This large loss of energy from ELMs appears distinctive to NSTX, as typical type I ELM stored energy loss on conventional devices is on the order of 10%. Additionally, type I ELMs on conventional tokamaks are generally accompanied by a loss of particles from the pedestal and edge regions, with the impact on the pedestal electron temperature (T_e) varying by machine.[8] However, on NSTX, these giant ELMs induce a large loss of electron energy corresponding to a drop in T_e over a large portion of the plasma, and a corresponding outflow of electron heat into the SOL and divertor region. These large transient heat loads would be problematic for high-power burning plasma machines, and they would quickly erode or destroy the PFC and divertor components regardless of their material composition. Therefore, it is imperative to understand the nature of these events and determine if they are unique to low-aspect-ratio geometry, and if they might play a role in the high-performance regimes for upcoming burning plasma devices.

This work will focus on the comparison between the "typical" type I ELM and the "giant" ELM on NSTX, and will attempt to demonstrate that one of the primary differences between the two is the electron thermal response of the plasma to the ELM perturbation. The destabilization of the

[a)]Paper NI1 5, Bull. Am. Phys. Soc. **52**, 188 (2007).
[b)]Invited speaker.

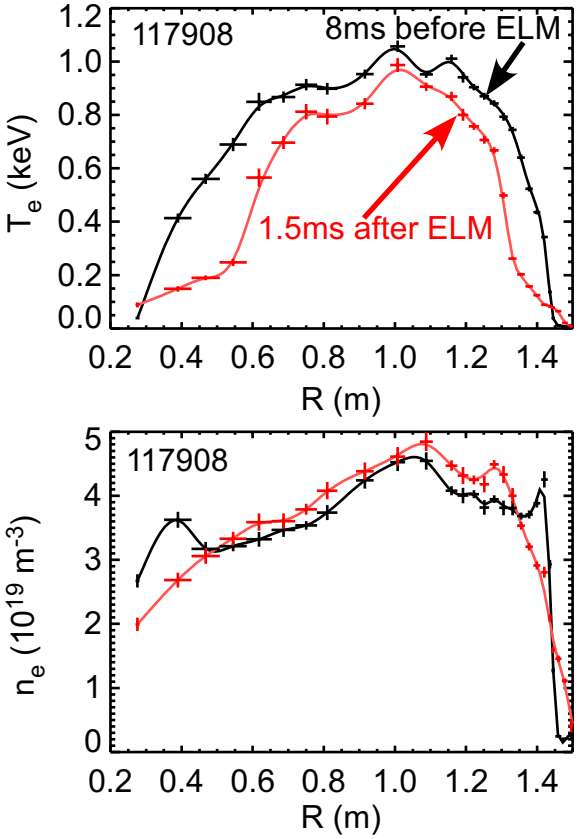

FIG. 1. (Color online) Thomson scattering snapshots of T_e and n_e profiles 8 ms before (black) and 1.5 ms after (red [gray]) a "giant" ELM showing a global decrease in the T_e profile.

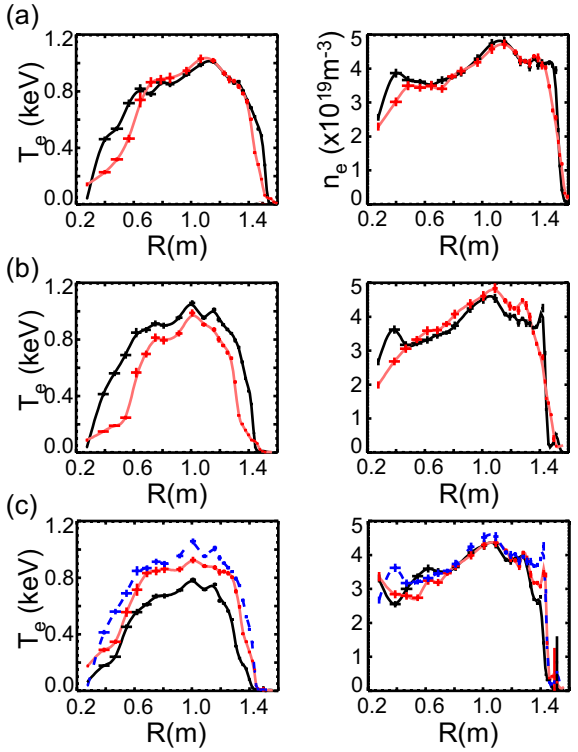

FIG. 2. (Color online) Sequence of Thomson scattering snapshots showing (a) initiation of cold pulse at the plasma edge (pre-ELM: black, start of cold pulse: red [gray]), (b) extension of the cold pulse to near the magnetic axis (pre-ELM: black, cold pulse: red [gray]), and (c) increase of the profiles to "pre-ELM" levels during a recovery phase (end of cold pulse: black, profile recovery: red [gray], pre-ELM level: blue [dashed]).

ELM itself, its specific character, and the various regimes and modes of operation are not addressed in detail, but are discussed in the previously mentioned references.

II. THE "GIANT" ELM

On NSTX, "giant" ELMs have been observed primarily in lower single null (LSN) diverted discharges with low pedestal collisionality ($\nu^* < 1$), and they are often interspersed with the more benign type V ELMs mentioned previously. The features of these large events have been characterized using Thomson scattering "snapshots" of the T_e and electron density (n_e) profiles, which demonstrate that the loss in W_{tot} corresponds to a global decrease in the T_e profile. Figure 1 shows the T_e and n_e profiles ~8 ms before and ~1.5 ms after a "giant" ELM. Between the two time slices, the T_e profile exhibits a nearly uniform drop extending close to the center of the discharge while n_e is affected only near the plasma edge. The drop in edge n_e corresponds to a loss of the density "ears" that are generated by the accumulation of a significant impurity fraction, usually carbon. In contrast, discharges with a small edge impurity fraction show little change of n_e during these ELMs, indicating that the drop in stored energy corresponds with a loss of electron thermal energy.

Piecing together profile snapshots taken during "giant" ELMs from comparable plasma discharges completes the picture of the profile dynamics. A snapshot 250 μs from the start of the ELM already shows the loss of the impurity density "ears" along with evidence that a cold pulse corresponding to the drop in T_e is initiated at the plasma edge [Fig. 2(a)]. In the next T_e profile snapshot, measured at a time 1.5 ms from the beginning of the ELM, the cold pulse has propagated to r/a ~0.2, close to the magnetic axis, while the global n_e remains constant [Fig. 2(b)]. Figure 2(c) shows T_e and n_e profiles 3, 13, and 33 ms from the beginning of the event, which illustrates the full extent of the T_e crash ($\Delta T_{e0}/T_{e0} \sim 30\%$) and the subsequent profile recovery to the pre-ELM level. During the profile recovery phase, we again see the buildup of the density profile "ears" as the impurities begin to reaccumulate in the plasma edge.

Because the ELMs are naturally intermittent and difficult to predict, T_e and n_e snapshots using the Thomson scattering system are unable to provide a detailed, continuous time history of the ELM event and its perturbation. Therefore, a time-resolved characterization of the ELM and corresponding cold pulse was obtained using soft-x-ray (SXR) emission measurements, which are sensitive to T_e, n_e, and impurity concentration. The SXR system on NSTX is comprised of a set of poloidally viewing diode arrays that view the plasma at one toroidal angle through an interchangeable filter set.[9] The poloidal system is complemented by a tangentially viewing "mutlicolor" optical SXR array that simultaneously samples the same plasma volume using three beryllium filters with different thicknesses (10, 100, and 300 μm).[10] The "multicolor" feature of this diagnostic allows the determina-

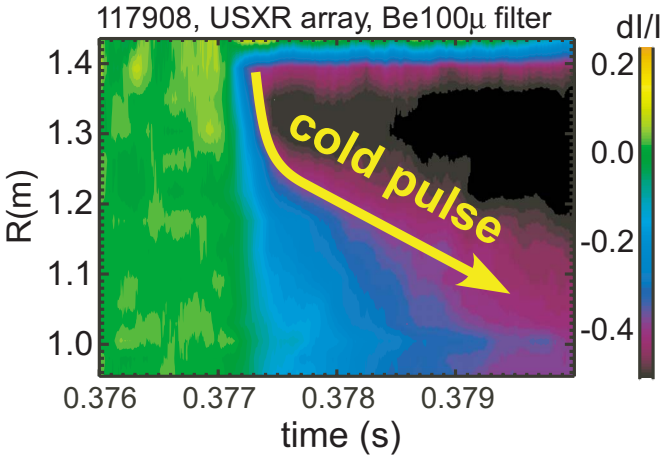

FIG. 3. (Color online) Relative SXR intensity showing cold pulse propagation during a "giant" ELM.

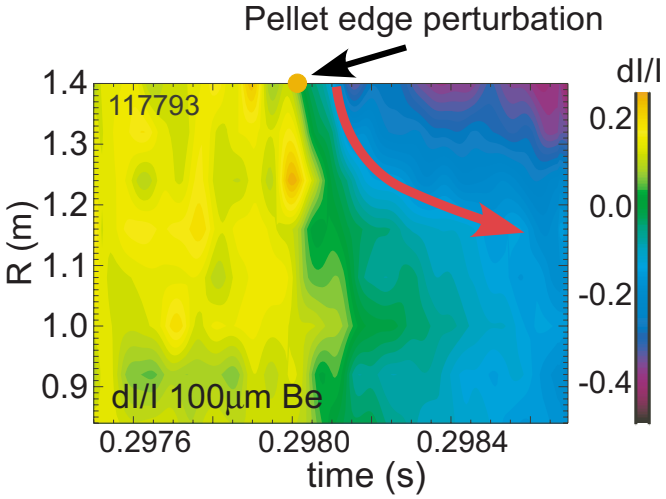

FIG. 4. (Color online) Relative SXR intensity showing cold pulse initiated by LPI into the "giant" ELM regime.

tion of the temperature, density, and impurity sensitivity of the measured SXR emission, thus providing a reconstruction of the T_e profile on a ~0.1 ms time scale while the tangential view allows an Abel inversion of the line-integrated data to obtain localized measurements.[11] Furthermore, this method takes advantage of the relatively clean, low-Z_{eff} nature of the NSTX plasmas by modeling and fitting to spectrally integrated x-ray emission calculated using the CHIANTI x-ray code.[12,13] The T_e, n_e, and impurity profiles are specified before the ELM using measured quantities. Then, the changes in the line integrated SXR intensities are used as a constraint to fit the calculated spectrally integrated emission using perturbed profiles until the result that best matches the data is obtained. The multicolor filter set provides a strong constraint on the electron temperature by providing a coarse energy subsampling of the continuum spectrum, while the spectral contributions from low-Z impurity line emission are suppressed by a proper choice of filters. Given the relative stability of the n_e profile over the bulk of the plasma, even a measurement of the relative SXR intensity provides insight into the cold pulse propagation. Figure 3 shows the relative SXR intensity from a poloidal array during a "giant" ELM. The time-resolved picture confirms the Thomson measurements; a cold pulse is initiated at the plasma edge, and propagates to the plasma core within a few ms.

Given the magnitude and global extent of the induced perturbation, an immediate question is whether the T_e crash is initiated by a small edge perturbation, or whether there is a large, global mode that is responsible for the fast loss of plasma stored energy. Observations of reconnections and other large magnetohydrodynamic (MHD) events show redistribution of the temperature and density on time scales faster than the perturbation associated with the "giant" ELM. The global constancy of the n_e profile indicates that the energy loss is through the electron thermal channel, rather than from large-amplitude MHD activity. Moreover, there is no evidence of related large coherent MHD activity either from the magnetic pickup sensors or from the SXR system, which is quite sensitive to internal plasma MHD modes (e.g., internal reconnection events).

To verify this hypothesis, small lithium pellets were injected into the edge of discharges in the "giant" ELM regime, exhibiting results that closely matched the behavior of the large ELMs (Fig. 4). The resultant perturbation caused a fractional drop in stored energy ($\Delta W_{\text{tot}}/W_{\text{tot}}$) of ~25%. Thomson scattering T_e and n_e profiles before and after the injection again showed a global crash in the T_e profile with a globally stable n_e profile. However, with lithium pellet injection (LPI) the impurity "ears" remained intact as the pellet did not trigger an ELM and the associated expulsion of the edge impurities. The similarity in magnitude and time scales of the induced cold pulse between the "giant" ELM and LPI indicates that the dynamics of the plasma response are governed by a large enhancement of the electron thermal transport, rather than by the type of the initiating edge perturbation.

A comparison to ordinary type I ELM behavior supports this deduction. Type I ELMs occur in discharges that tend to be more highly shaped and closer to the double null diverted (DND) configuration, with a much smaller ELM energy loss, $\Delta W_{\text{tot}}/W_{\text{tot}} \sim 4-10\%$.[14] The corresponding cold pulse is smaller in amplitude, and propagates more slowly into the core on time scales of several ms [Fig. 5(a)]. Additionally, the core plasma in type I ELM discharges showed little sensitivity to the LPI perturbation, with the plasma response limited to plasma edge [Fig. 5(b)]. The variations in cold pulse behavior and response to pellet injection suggest that one of the primary differences between the "giant" ELM and type I ELM regime is the enhancement of the plasma electron thermal transport, χ_e, due to an edge perturbation. The inferred large χ_e^{enh} during the "giant" ELM evolution is thus responsible for the decline in the global T_e profile and corresponding large $\Delta W_{\text{tot}}/W_{\text{tot}}$. Parameters comparing the two plasma regimes are provided in Table I.

Though many of the discharge parameters are similar, the ELM behavior changes from the "giant" perturbations to the more typical type I ELMs as the plasma shape changes from the LSN, higher elongation lower triangularity shape to a plasma closer to a DND configuration ($dr_{\text{sep}} \sim 0$) with

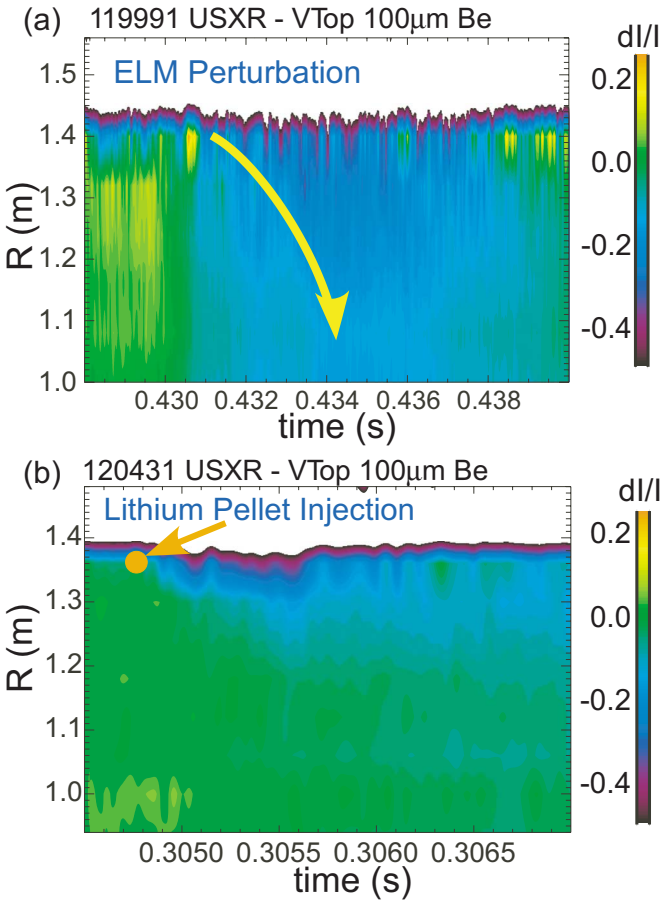

FIG. 5. (Color online) Relative SXR intensity showing plasma response to (a) type I ELM and (b) LPI injection into the type I ELM regime.

higher triangularity. The high voltage of the neutral beams (~90 keV) compared with the typical T_{e0} (~1 keV) indicates that the injected neutral beam power (P_{NB}) predominantly heats the electrons. Calculations from the TRANSP code[15] show that in both cases, ~50% of P_{NB} goes to electron heating, ~25% goes to the ions, and ~25% is accounted for via fast ion losses and other mechanisms.

TABLE I. Comparison of machine and discharge parameters for the "giant" ELM and the type I ELM regime.

Parameter	"Giant" ELM	Type I ELM
I_p (MA)	1.0	1.0
B_{T0} (T)	0.45	0.45
P_{NB} (MW)	4	4–6
R_0 (m)	0.86	0.85
A	1.36	1.34
q_{95}	9	8.5
κ	2.0	1.8
δ_{up}, δ_{down}	0.35, 0.48	0.48, 0.53
dr_{sep} (m)	–0.02	–0.004
β_T (%)	15	13
l_i	0.6	0.7

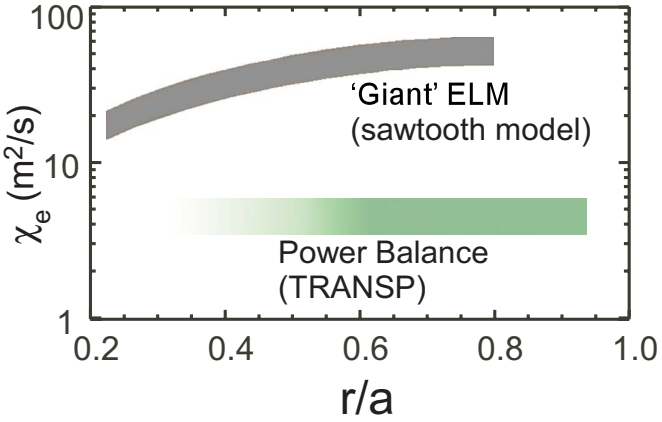

FIG. 6. (Color online) Comparison of χ_e^{enh} during a "giant" ELM, deduced from calculated fast T_e profiles, to the steady-state power balance χ_e from the TRANSP code.

III. TRANSPORT ANALYSIS

The enhanced electron transport indicated during "giant" ELMs is studied using the sawtooth heat-pulse model to calculate a diffusive, enhanced χ_e^{enh} from the "time-to-peak" measurements of the heat pulse radial location. The following equation[16] is used:

$$\chi_e^{enh} \approx \frac{\Delta r_{eff}^2}{8\Delta t_{peak}}, \quad (1)$$

where r_{eff} is the minor radius based on the effective area of the flux surface. For these highly shaped NSTX plasmas with a significant Shafranov shift, $\Delta r_{eff}^2 \approx 4\Delta r^2$, where Δr is the distance of the cold pulse front from the outboard edge of the plasma. Even though the underlying physics of the fast cold pulse propagation appears to be nonlinear, the relative impact of the enhanced transport on the temperature profile will be studied by comparing the steady-state power balance χ_e generated by the TRANSP code to the effective diffusive χ_e^{enh} generated by the sawtooth model. Though this simplified model is unlikely to capture all of the relevant transport physics, it allows a qualitative comparison to demonstrate the dramatic increase in the perturbed χ_e^{enh} over the underlying power balance χ_e.

The enhanced electron thermal transport for a "giant" ELM cold pulse is shown in Fig. 6. The time-to-peak values were obtained using a time-resolved calculation of the T_e profile from the "multicolor" SXR array mentioned previously. As shown in the figure, the estimated χ_e^{enh} is an order of magnitude higher than the power balance χ_e calculated from TRANSP, which is consistent with the rapid loss of electron thermal energy during the propagation of the cold pulse. Additionally, the enhanced transport is higher toward the plasma edge in the large ∇T_e region, and is lower in the plasma core where the T_e profile is nearly flat. Conversely, the estimated χ_e^{enh} during an ordinary type I ELM perturbation is similar in value to the power balance χ_e calculated from TRANSP of a few tens of m^2/s across the plasma minor radius, suggesting that the perturbation from a normal type I ELM propagates through the plasma at a rate governed by the underlying anomalous electron thermal transport. Though

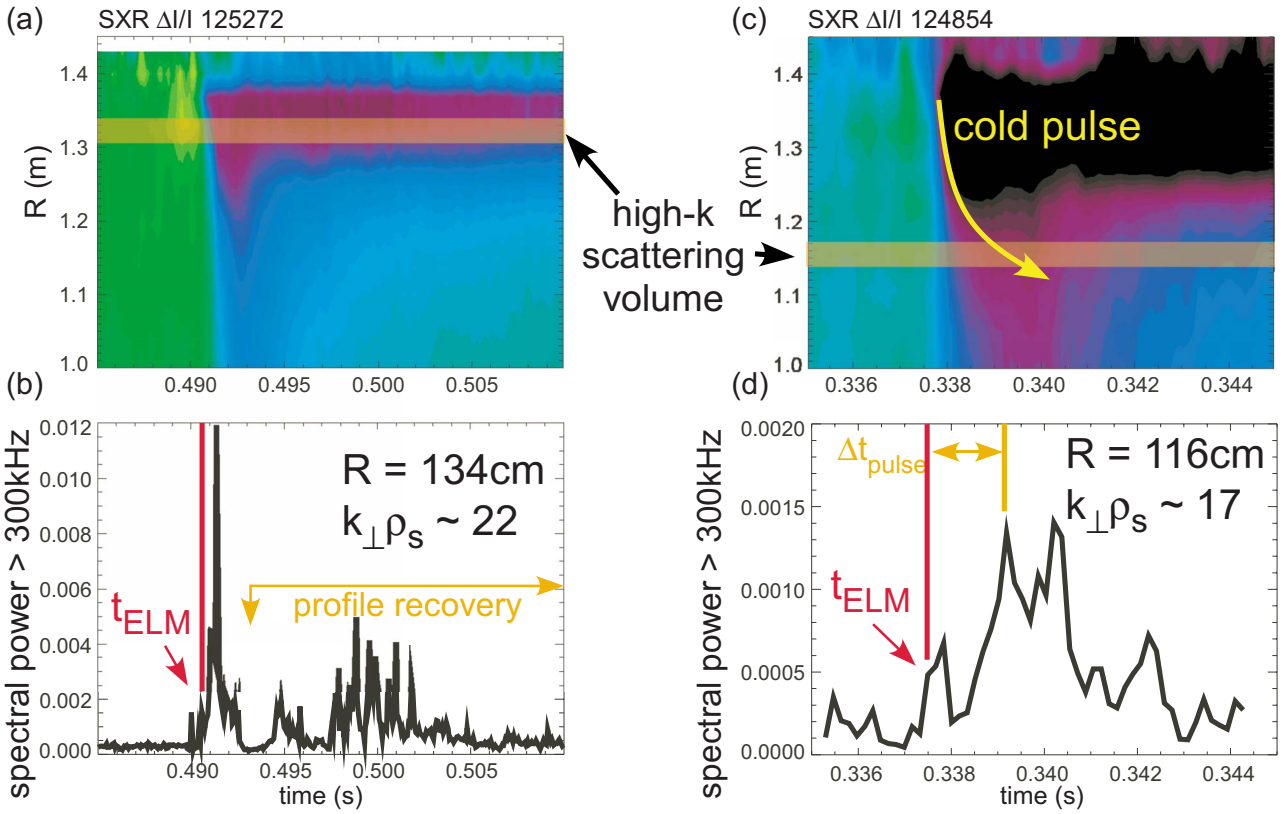

FIG. 7. (Color online) (a) Relative SXR intensity during a "giant" ELM with (b) corresponding high-k fluctuation measurements at $R \sim 134$ cm. (c) Relative SXR intensity during a "giant" ELM with (d) corresponding high-k fluctuation measurements at $R \sim 117$ cm.

the cause and exact nature of this steady-state anomalous electron transport is unknown, current theories predict that microtearing instabilities can play an important role in NSTX plasmas, and have generated χ_e values consistent with observations.[17]

Given the difference in transport in these two regimes, it is natural to search for additional evidence of increased transport by looking at the magnitude of plasma fluctuations before, during, and after the "giant" and type I ELMs. Two other features of the "giant" ELM perturbation, namely the loss of energy through the electron heat channel and the approximate scaling of χ_e^{enh} with ∇T_e, suggest that the enhanced electron thermal transport could be driven by the destabilization of electron temperature gradient (ETG) modes. These modes should be observable as short-wavelength, high-k density fluctuations.[18] Another candidate instability for driving the loss of electron thermal energy is the trapped electron mode (TEM),[19] which shares many of the same stability characteristics of the ETG mode, though the TEM operates at lower k, and outside the range of measurements on NSTX. Nonetheless, a discussion and comparison of the ETG and TEM instabilities in Sec. V will show that the TEM is predicted to be stable in these discharges.

IV. FLUCTUATION MEASUREMENTS

The high-k scattering system on NSTX measures short-wavelength fluctuations by collecting the signal from a 280 GHz probe beam that is coherently scattered from density variations with a high radial wavenumber, k_r.[20] The system has multiple collecting channels for a simultaneous measurement of the fluctuation spectrum over a range of k_r from 4 to 24 cm^{-1}. The high-k measurement volume has a radial spatial resolution of $+/-3$ cm, and can be scanned across the outboard plasma minor radius between plasma discharges. Fluctuation measurements were collected for both the "giant" ELM and the type I ELM near the plasma core ~ 117 cm, $r/a \sim \sqrt{\phi_n} = 0.2$, and closer to the plasma edge ~ 134 cm, $r/a \sim \sqrt{\phi_n} = 0.5$.

Figure 7 shows the cold pulse as measured by the relative SXR signal and the corresponding high-k fluctuations near the edge and in the core for a "giant" ELM. The edge fluctuations increase dramatically, coincident with the ELM onset, and persist for the duration of the cold pulse propagation. The edge fluctuations subside at the start of the profile recovery, but exhibit intermittent bursts of short-wavelength activity during the profile recovery phase. The increase in core high-k fluctuations exhibits a time delay of ~ 1.5 ms, which corresponds to the time it takes for the cold front to propagate from the edge to the measurement location at 117 cm. The cold front is a region of higher T_e gradient, which is sufficient to destabilize the short-wavelength fluctuations in the plasma core.

In both the edge and core fluctuation measurements, there is a short, initial spike that corresponds to the beginning of the ELM. This brief increase in amplitude is related to a broadband increase of the scattered signal over the range of measured k and is unlikely to be correlated with actual short-wavelength fluctuations, though its exact cause is not

yet determined.[21] Such spurious broadband signals can be differentiated from high-k fluctuation measurements, which generally exhibit broad spectral features peaking at a nonzero central frequency. In fact, core and edge high-k measurements during a normal type I ELM show only this spurious initial spike, and no increase in fluctuation levels during the corresponding cold pulse. This supports the hypothesis that the propagation progresses at the rate of the underlying transport, contrary to the enhanced transport induced by the "giant" ELM.

V. COMPARISONS TO LINEAR STABILITY THEORY

The existence of high-k fluctuations during the "giant" ELM cold pulse is supported by linear stability calculations, which predict ETG destabilization for the location and times of interest. At the edge, the results of GS2 linear stability calculations[22] indicate strong destabilization of modes in the ETG range from $k_\theta \rho_s \sim 12-50$. These modes are predicted to be stable before the ELM (Fig. 8). These short-wavelength modes are also predicted to be stable for the normal type I ELM case, which is consistent with the lack of high-k fluctuations and lower transport of the corresponding cold pulse.

Also of note are the calculated growth rates for the TEM instabilities. In fact, the larger spatial scales of the TEM suggest that their destabilization could play an important, if not dominant, role in the observed enhanced thermal transport during an ELM. However, the calculated ExB shearing rate for the times of interest range from ~0.3 Mrad/s near the core to ~3 Mrad/s close to the plasma edge, which far exceeds the calculated growth rates of the TEM and lower-k instabilities. Though the shearing rate is on the order of the calculated growth rates for the ETG modes, the small spatial scales of the high-k instability eliminate the effectiveness of flow shear stabilization for the ETG mode.[18] Additionally, the global stability of the density profile during the cold pulse perturbations indicates no increase in electron particle flux that often accompanies the TEM instability.

The short-wavelength fluctuations are predicted to be initially stable in the core of the plasma due to the relatively flat T_e profile. Using the fast T_e capability of the "multicolor" SXR system, the T_e profile was computed throughout the cold pulse (Fig. 9), allowing a calculation of the normalized electron temperature gradient, R/L_{Te}. The value of R/L_{Te} increased from ~1.5 to ~2.5, which is in the range of values predicted for destabilization using an analytic approximation of the ETG linear stability critical gradient threshold, $(R/L_{Te})_{\text{crit}}$, given by the following relationship:[23]

$$(R/L_{Te})_{\text{crit}} = \max\{(1+\tau)(1.33+1.91\hat{s}/q)(1-1.5\varepsilon) \times[1+0.3\varepsilon(d\kappa/d\varepsilon)], 0.8R/L_n\}, \quad (2)$$

where $\tau = Z_{\text{eff}}(T_e/T_i)$ is an impurity term, $\hat{s}$ is the magnetic shear $r/q(dq/dr)$, q is the safety profile, ε is the inverse aspect ratio, κ is the elongation, and R/L_n is the normalized density gradient. The calculation for this discharge at the high-k measurement location was done with local values of $\hat{s} \sim 0.3$ and $\varepsilon \sim 0.33$, which are close to the limits of validity for the above expression. The value of $(R/L_{Te})_{\text{crit}}$ was 2.7 from a GS2 calculations for these profiles, matching the analytic approximation. The time scale of the growth of the high-k fluctuation amplitude in the core agrees with the predicted time at which the computed R/L_{Te} reaches $(R/L_{Te})_{\text{crit}}$, 1.5 ms after the ELM onset (Fig. 10).

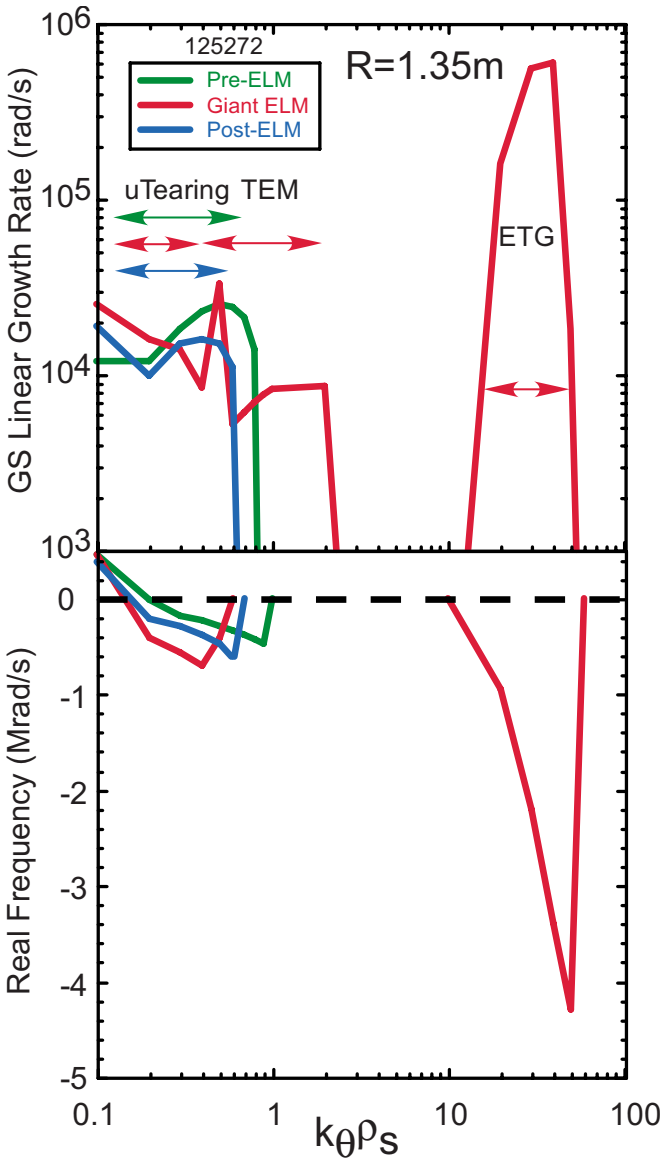

FIG. 8. (Color online) Linear stability calculation using GS2 showing destabilization of ETG modes during a "giant" ELM and high-k stability in the type I ELM regime.

The increase in fluctuations during a "giant" ELM cold pulse along with the theoretical indications of short-wavelength destabilization strongly suggest that the large reduction in plasma stored energy, and indications of enhanced electron thermal transport, are due to the destabilization of ETG modes. Even in the initially stable plasma core, the T_e gradient accompanying the cold pulse results in a predicted and observed destabilization of high-k fluctuations. This contrasts with the response to a type I ELM, which is both observed and predicted to be stable to short-wavelength instabilities.

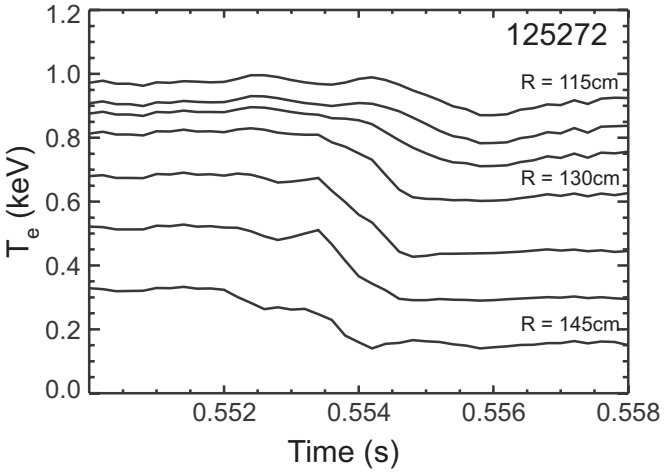

FIG. 9. Calculated T_e at various radii during a "giant" ELM.

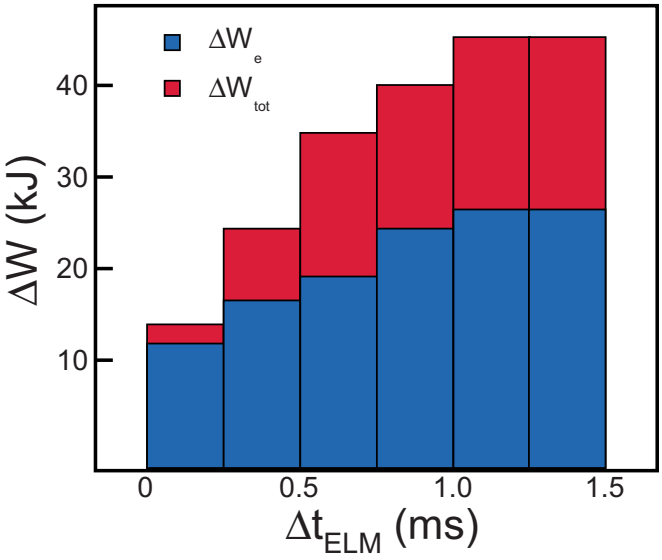

FIG. 11. (Color online) Calculation of loss of thermal electron energy compared to total stored energy loss during a "giant" ELM.

VI. CONCLUSIONS

Of the variety of ELM behavior observed on NSTX, the energy loss from the "giant" ELM of $\Delta W_{\mathrm{tot}}/W_{\mathrm{tot}} \sim 30\%$ poses a particularly serious issue if this large perturbative phenomenon occurs in future, high-power fusion devices. Thomson scattering measurements show that this large energy loss corresponds with a global drop in the T_e profile, corresponding to the initiation of a cold pulse that travels from the edge to the core on the time scale of a few ms. The change in T_e profile, along with the characterization of the cold pulse propagation, indicates a strong enhancement of the electron thermal transport. This enhanced transport correlates with a dramatic increase in short-wavelength, high-k fluctuations in both the edge and core regions of the plasma, and its onset agrees with the time of destabilization of ETG modes as predicted by linear stability theory. This behavior contrasts with the typical type I ELM perturbation, which is both predicted and observed to be stable to high-k fluctuations, and tends to propagate inward at the underlying anomalous electron thermal transport rates.

The baseline underlying transport is not yet fully understood on NSTX, especially at low-k wavelengths, as no corresponding measurement is available. The response of the ions is also not well characterized, though again the large ExB shear is predicted to stabilize the ITG mode. The T_i profile is substantially lower after a "giant" ELM, but the 10 ms response time of the measurement prevents a fast assessment.[24] However, a decrease in T_i would be expected merely from increased ion-electron thermal coupling during a cold pulse due to the lower T_e,[25]

$$\tau_{ie} \propto T_e^{-3/2} \Rightarrow \tau_{ie} \leqslant 1 \text{ ms}. \tag{3}$$

Thus, the T_i profile should decrease on time scales much faster than the time resolution of the T_i measurement, and on the same time scale as the propagation of the cold pulse. Therefore, even with fast T_i measurements, separation of the ion thermal losses through coupling to the electron channel from loss because of enhanced ion thermal transport is challenging. Nonetheless, a comparison of the change in electron energy with the change in total stored energy shows that the drop in energy immediately following the ELM is almost entirely from the electrons (Fig. 11). During the cold pulse, both the total stored energy and the electron thermal energy continue to drop, though the proportionally smaller fraction of electron energy indicates that the ion energy loss is increasing on the expected time scales.

An additional missing piece of information is the response of the plasma at low-k wavelengths. Cascades and energy transfers between the low- and high-k regions of the fluctuation spectrum could play an important part of the plasma response during "giant" ELM perturbations, and reliable projections to future devices will require a more complete understanding of this phenomenon.

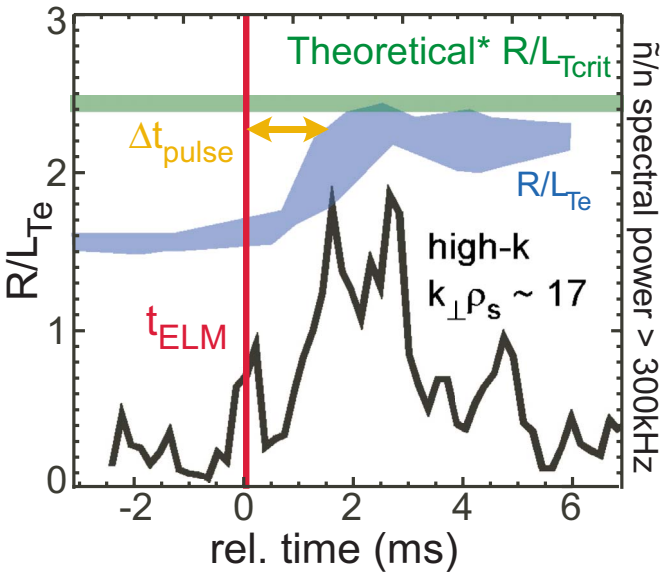

FIG. 10. (Color online) Calculation of R/L_{Te} and comparison to measurement of high-k fluctuations in the core, $R \sim 117$ cm, during a "giant" ELM cold pulse.

ACKNOWLEDGMENTS

The authors appreciate and acknowledge the assistance from the NSTX support staff, machine operators, neutral beam operators, and the research team. CHIANTI is a collaborative project involving the NRL (USA), RAL (UK), MSSL (UK), the Universities of Florence (Italy) and Cambridge (UK), and George Mason University (USA).

This research is supported by DOE Grant No. DE-FG02-99ER5452.

[1] M. Becoulet, G. Huysmans, Y. Sarazin *et al.*, Plasma Phys. Controlled Fusion **45**, A93 (2003).
[2] A. Loarte, G. Saibene, R. Sartori *et al.*, J. Nucl. Mater. **313–316**, 962 (2003).
[3] G. Federici, A. Loarte, and G. Strohmayer, Plasma Phys. Controlled Fusion **45**, 1523 (2003).
[4] J. Menard, M. G. Bell, R. E. Bell *et al.*, Nucl. Fusion **47**, S645 (2007).
[5] R. Maingi, K. Tritz, E. D. Fredrickson *et al.*, Nucl. Fusion **45**, 264 (2005).
[6] R. Maingi, C. E. Bush, E. D. Fredrickson *et al.*, Nucl. Fusion **45**, 1066 (2005).
[7] C. E. Bush, M. G. Bell, R. E. Bell *et al.*, Phys. Plasmas **10**, 1755 (2003).
[8] D. N. Hill, in *LLNL Report UCRL-JC--124081* (LLNL, Livermore, CA, 1996), p. 52.
[9] D. Stutman, M. Finkenthal, H. W. Moos *et al.*, Rev. Sci. Instrum. **74**, 1982 (2003).
[10] L. F. Delgado-Aparicio, D. Stutman, K. Tritz *et al.*, Plasma Phys. Controlled Fusion **49**, 1245 (2007).
[11] L. F. Delgado-Aparicio, D. Stutman, K. Tritz *et al.*, J. Appl. Phys. **102**, 073304 (2007).
[12] E. Landi and M. Landini, Astron. Astrophys. Suppl. Ser. **133**, 15 (1998).
[13] E. Landi, G. Del Zanna, P. R. Young *et al.*, Astrophys. J., Suppl. Ser. **162**, 261 (2006).
[14] R. Maingi, S. A. Sabbagh, C. E. Bush *et al.*, J. Nucl. Mater. **337–339**, 727 (2005).
[15] R. J. Hawryluk, *Physics of Plasmas Close to Thermonuclear Conditions* (Commission of the European Communities, Brussels, 1981), Vol. 1, p. 19.
[16] M. Soler and J. D. Callen, Nucl. Fusion **19**, 703 (1979).
[17] K. L. Wong, S. Kaye, D. R. Mikkelsen *et al.*, Phys. Rev. Lett. **99**, 135003 (2007).
[18] W. Dorland, F. Jenko, M. Kotschenreuther *et al.*, Phys. Rev. Lett. **85**, 5579 (2000).
[19] T. Dannert and F. Jenko, Phys. Plasmas **12**, 072309 (2005).
[20] D. R. Smith, E. Mazzucato, T. Munsat *et al.*, Rev. Sci. Instrum. **75**, 3840 (2004).
[21] H. Park, personal communication (2007).
[22] M. Kotschenreuther, G. Rewoldt, and W. M. Tang, Comput. Phys. Commun. **88**, 13 (1995).
[23] F. Jenko, W. Dorland, and G. W. Hammett, Phys. Plasmas **8**, 9 (2001).
[24] D. Johnson and N. Team, Plasma Phys. Controlled Fusion **45**, 1975 (2003).
[25] J. Wesson, *Tokamaks* (Oxford University Press, New York, 2004).